J. Plasma Phys. (2023), *vol*. 89, 955890302
Published by Cambridge University Press

doi:10.1017/S0022377823000417

Overview of core impurity transport in the first divertor operation of Wendelstein 7-X

Th. Wegner [1],†, J.-P. Bähner [1],‡, B. Buttenschön [1], A. Langenberg [1], A. von Stechow [1] and the W7-X Team [1],§

[1]Max-Planck Institute for Plasma Physics, 17491 Greifswald, Germany

(Received 27 October 2022; revised 5 April 2023; accepted 5 April 2023)

The impurity transport at Wendelstein 7-X during its most recent campaign is characterized and documented for a variety of different plasma scenarios. An overview of its dependence on several quantities is given, which allows identification of transport regimes and the major driver for impurity transport. Beyond this, a comparison with the impurity behavior in other fusion devices is now possible. In contrast to other stellarators, no density dependence of the impurity transport has been found. Additionally, the influence of the turbulence contribution to the overall transport is reflected in the dependence on various parameters, e.g. turbulent diffusion and density fluctuation amplitudes. With this database approach, one can now also apply scaling laws to make extrapolations about the impurity confinement in future plasma scenarios.

Key words: fusion plasma, plasma confinement, plasma diagnostics

1. Introduction

The Wendelstein 7-X (W7-X) stellarator (Klinger *et al.* 2019) is designed for long pulse steady state plasma operation. Hence, the control and improvement of the overall performance is a major task in fusion research. Intrinsic impurities being released from plasma facing components during plasma–wall interaction or released as a product during the fusion reaction can dilute the plasma, degrade the energy confinement and limit accessible operational parameter ranges. The radiation of these impurities in the plasma reduces the plasma temperature and might lead to radiative instabilities. Hence, impurity accumulation has to be avoided since its massive presence can significantly degrade the plasma performance of a fusion device (Ida *et al.* 1987). For these reasons, the investigation of the impurity transport is of utmost importance.

There are several studies reporting on impurity confinement in W7-X (Geiger *et al.* 2019; Langenberg *et al.* 2020, 2021; Wegner *et al.* 2020*a*; García-Regaña *et al.* 2021*b*), however, these works focus only on individual plasma scenarios without giving an overview considering different plasma conditions. However, in order to achieve a uniform

† Email address for correspondence: thomas.wegner@ipp.mpg.de, physics@thwegner.com
‡ Present address: MIT Plasma Science and Fusion Center, Cambridge, MA 02139, USA
§ Author list in T. Sunn Pedersen et al. Nucl. Fusion **62**, 042022 (2022)

and consistent understanding of impurity behavior, an overview is of great importance and is presented in the following.

After an introduction of the analyzed scenarios and methodology in § 2, the dependence of the impurity confinement behavior on different parameters is presented in the subsequent § 3. Finally, § 4 summarizes the most important results and motivates the further application of the database created in the framework of this work.

2. Analyzed scenarios and methodology

The objective of this study is the characterization and documentation of the core impurity transport at W7-X at a variety of different plasma conditions. Therefore, 52 experimental programs at different plasma parameters are considered in the following. The experiments were performed in the previous operational phase (OP1.2b with uncooled carbon divertor) in two different magnetic field configurations ('standard' and 'high mirror' labelled as EJM and KJM Andreeva 2002) using hydrogen as the main fuel gas. In these experimental programs, a total of 123 (64 in EJM and 59 in KJM) non-intrinsic impurity injections were applied by means of the laser blow-off (LBO) system (Wegner *et al.* 2018, 2020). In particular, trace amounts of iron (less than 10^{17} atoms and $n_{\mathrm{Fe}}/n_{\mathrm{e}} < 10^{-5}$) were injected into different plasma scenarios. An overview of the parameter space is shown in figure 1.

It should be emphasized that all of the following conclusions and scaling attempts are based on this database. This database represents the most relevant operational regimes during the considered campaign. However, in order to allow a reliable evaluation of the impurity transport, only experimental programs at stationary conditions are included. Most of them were performed in pure electron cyclotron resonant heated (ECRH) plasmas. In addition, a few discharges with neutral beam injection (NBI) heating of up to 3.5 MW on top of ECRH power are also taken into account for the following analysis.

The methodology consists of studying the impurity transport and its dependence on other quantities to examine transport regimes and allow predictive statements. Hence, the above mentioned impurity injection by means of LBO is evaluated in terms of the impurity transport time τ_I, being a measure for the impurity confinement. The transport time is the decay time of the spectroscopic signals in the vacuum ultraviolet (VUV) and X-ray wavelength range, taking into account various charge stages of iron. Additionally, the transport coefficients are inferred by a one-dimensional transport code STRAHL (Behringer 1987). Further details of this analysis are described in the literature (Wegner *et al.* 2018; Geiger *et al.* 2019; Wegner *et al.* 2020*a*).

Due to experimental and numerical confirmation of a large diffusive turbulent contribution to the impurity transport (e.g. flat impurity profiles) in standard ECRH plasmas (dominant ECRH without kinetic profile shaping events, e.g. pellet injection) (Geiger *et al.* 2019; Langenberg *et al.* 2020; Wegner *et al.* 2020*a*; García-Regaña *et al.* 2021*a*,*b*), only the inferred diffusion coefficient is considered in the following study. In particular, the turbulent diffusion profile is inferred using an iterative optimization procedure embedded in STRAHL while the convection profile is set to the classical and neoclassical estimations. A comparable determination of the turbulent convection profile is too inaccurate with the current data situation and, as mentioned above, is not necessary for most of the plasma scenarios presented here.

The following discussion includes not only the transport parameters but also the Thomson scattering data (Pasch *et al.* 2016), such as the electron density and temperature profiles (n_{e}, T_{e}), as well as the measurements from the X-ray imaging spectroscopy (Langenberg *et al.* 2017) with respect to the ion temperature profile (T_{i}). These profiles are used as input to evaluate the classical and neoclassical transport parameters

https://doi.org/10.1017/S0022377823000417 Published online by Cambridge University Press

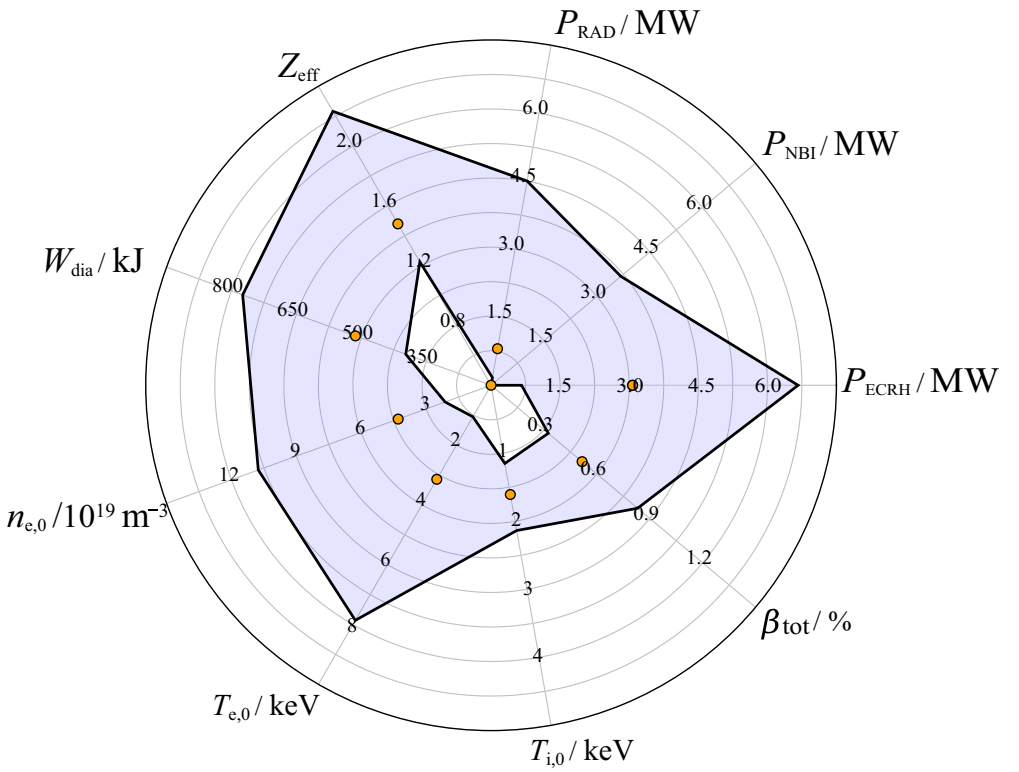

FIGURE 1. Overview of the parameter space of the ECRH power P_{ECRH}, NBI heating power P_{NBI}, radiated power P_{RAD}, effective ion charge Z_{eff}, diamagnetic energy W_{dia} as well as the central values of the electron density $n_{e,0}$, electron temperature $T_{e,0}$ and ion temperature $T_{i,0}$ and the plasma beta β_{tot}, respectively. The filled circles within the individual parameter space indicate the median of the interval.

(D_{neo}, v_{neo}) with the drift kinetic equation solver (DKES) (Hirshman *et al.* 1986). In addition, the density fluctuation amplitude ($\tilde{n}_e$) measured with the phase contrast imaging (PCI) system (Edlund *et al.* 2018) is incorporated into the following discussion. To achieve comparability to other discharges, the density fluctuation amplitude is normalized to the line-integrated electron density.

3. Results and discussion

The correlation of the transport properties to the above mentioned parameters and the attempt to derive scaling laws from them enables a direct comparison with other machines and allows an extrapolation of the impurity transport in future plasma scenarios.

The behavior of the impurity confinement in terms of dependence on the main plasma parameters is shown in figure 2 using the transport time as a representative. Fortunately, the confinement of impurities in W7-X at moderate densities is fairly weak so far, which is reflected in relatively low transport times of the order of approximately 100 ms. Hence, most experimental programs could be conducted without any impurity accumulation. Nevertheless, there is one program that exhibits higher impurity confinement and for which transport times of up to 1 s have been observed. These are examined and discussed in more detail below.

https://doi.org/10.1017/S0022377823000417 Published online by Cambridge University Press

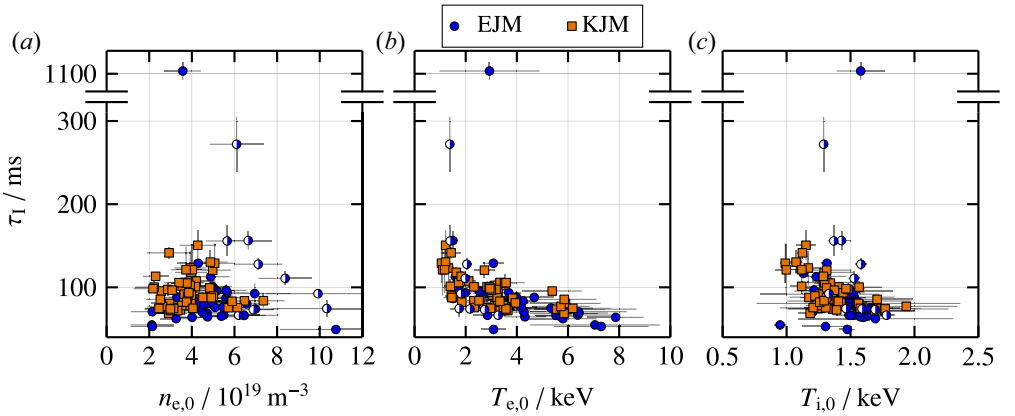

FIGURE 2. Impurity transport time over the central electron density (*a*) and temperature (*b*) as well as over the ion temperature (*c*) for the magnetic field configurations 'standard' (EJM, ○) and 'high mirror' (KJM, □). The main heating scheme is visualized with the filling degree of the symbols (half-filled: NBI and ECRH, full: pure ECRH).

At these moderate electron densities, a clear density dependence cannot be observed. However, there seems to be a general correlation between the impurity confinement and the electron temperature as the transport time decreases with higher temperatures. This suggests that the ECRH, which significantly determines the electron temperature, has an influence on the transport behavior. In the following it will be shown that the ECRH determines the level of turbulence. However, there is no clear correlation between the transport time and the core ion temperature. Additionally, there is no obvious difference in the impurity transport between the two magnetic field configurations EJM and KJM. This is particularly true for all parameters presented for comparison and dependency studies. This weak dependence on these two magnetic field configurations is basically expected and supported by theory, assuming the transport is dominated by turbulence (Langenberg *et al.* 2020; Navarro *et al.* 2020; Wegner *et al.* 2020*a*). Hence, it is planned to rather compare the magnetic field configurations 'low' and 'high mirror' since gyro-kinetic simulations presume a significant difference in the turbulent transport (Navarro *et al.* 2020).

In the following, the dependence on the magnetic field configuration is not further elaborated and presented in the figures. In addition, for the database considered here, no conclusive picture of the influence of heating deposition, plasma beta (plasma pressure normalized to magneticfield), electric field (beside core ion and electron root confinement) or rotational transform could be found, as has been observed in other papers (see the summary in Burhenn *et al.* 2009). One reason for this could be that the overall statistical analysis of many different plasma scenarios does not allow a direct comparison. For this, one would have to select dedicated experimental programs and investigate them in detail. However, this is not the focus of this paper and will be addressed in future publications. Furthermore, the parameter space and variation for some parameters, e.g. magnetic field strength or minor radius, is not large enough to conduct reliable dependency studies. The NBI heated scenarios are particularly conspicuous in the plots of electron density and ion temperature, see figure 2(*a*,*c*).

First, it must be mentioned that the NBI system is generally fuelling (density increase) as well as heating (ion temperature increase). Moreover, it it has been observed that the turbulent transport channel is suppressed in NBI heated plasmas, leading to higher transport times and hence better confinement (Romba *et al.* 2023). Since the ions are

https://doi.org/10.1017/S0022377823000417 Published online by Cambridge University Press

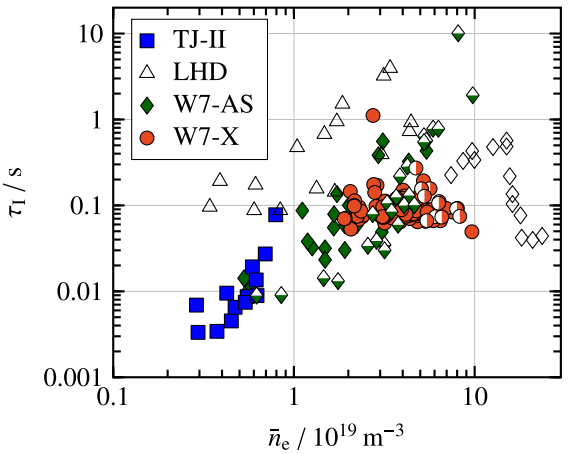

FIGURE 3. Impurity transport time over line-averaged density for the stellarators TJ-II* (□), LHD* (△), W7-AS* (◇) and W7-X (○). The main heating scheme is visualized with the filling degree of the symbols (empty: pure NBI, half-filled: NBI and ECRH, full: pure ECRH). *Data taken from Burhenn *et al.* (2009).

mainly heated via the electron-to-ion energy exchange power and due to the observed high core ion transport, the ion temperature is basically saturated below 2 keV (Beurskens *et al.* 2021).

With the electron density, a first rudimentary comparison with other stellarators is possible and is shown in figure 3. In particular, the transport time of impurities is plotted against the line-averaged density. Compared with other machines, again, the density dependence of the transport time for W7-X is rather small. Confinement changes as found for W7-AS at higher densities (transition from H to HDH mode) (Burhenn *et al.* 2009) could not be observed for W7-X up to now. Nevertheless, the confinement in W7-X is lower compared with the other stellarators above a line-averaged density of 5×10^{19} m^{-3}. In terms of impurities and their potential impact on the overall plasma properties, these are encouraging prospects, despite the fact that the energy confinement is also relatively low.

A more detailed view can be obtained by studying the transport behavior and, in particular, by determining the transport coefficients as mentioned in § 2. Obviously, there is a correlation between the transport time and the line-averaged diffusion coefficient, see figure 4. With the help of the inferred diffusion coefficient, the transport regime can be determined by relating it to the neoclassical diffusion values. Taking into account that a purely neoclassical transport leads to transport times of the order of seconds (Langenberg *et al.* 2020), the here observed transport times are below the neoclassical estimations. In particular, the observed diffusion coefficient is orders of magnitude larger compared with neoclassical (including classical contribution) expectations. Nevertheless, there seems to be some kind of threshold at a ratio of 100 between the turbulent and neoclassical diffusion. Below a ratio of 100, the transport time increases above 100 ms and the turbulent influence seems to reduce. If the ratio exceeds 100, the transport time decreases below 100 ms down to approximately 50 ms for turbulence enhanced scenarios.

All the above statements on the influence of turbulence on transport behavior have recently been discussed in experimental (Geiger *et al.* 2019; Langenberg *et al.* 2020; Wegner *et al.* 2020*a*) and theoretical (Helander & Zocco 2018; Alcusón *et al.* 2020; Wegner *et al.* 2020*a*; Xanthopoulos *et al.* 2020; García-Regaña *et al.* 2021*a*,*b*) works.

https://doi.org/10.1017/S0022377823000417 Published online by Cambridge University Press

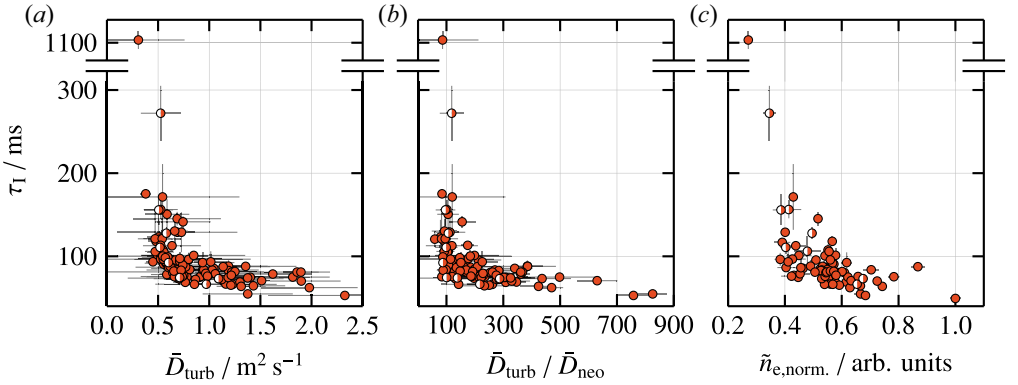

FIGURE 4. Impurity transport time over the line-averaged turbulent diffusion coefficient (*a*), the ratio between the turbulent and neoclassical line-averaged diffusion coefficient (*b*) and the normalized density fluctuation amplitude (*c*). The main heating scheme is visualized with the filling degree of the symbols (half-filled: NBI and ECRH, full: pure ECRH).

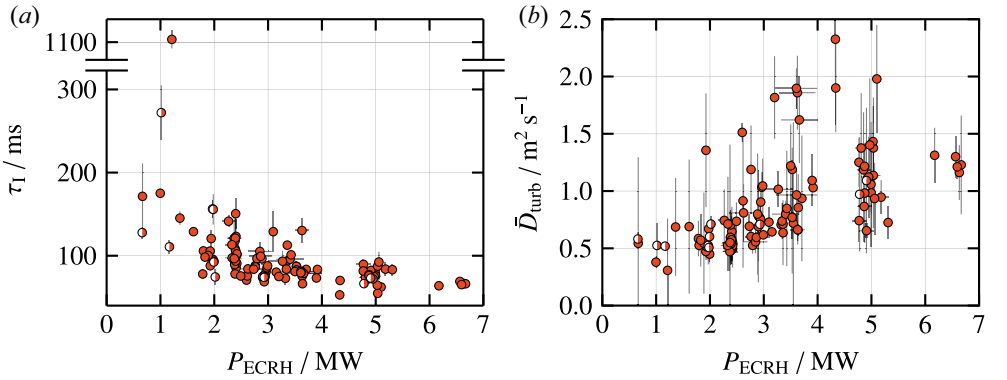

FIGURE 5. Impurity transport time (*a*) and the line-averaged turbulent (*b*) over the ECRH power. The main heating scheme is visualized with the filling degree of the symbols (half-filled: NBI and ECRH, full: pure ECRH).

Some experimental programs are compared with respect to their turbulence level (Wegner *et al.* 2020*a*), however, a comprehensive overview is still missing. An overview of the transport time and confinement is shown in figure 4(*c*) as a function of the density fluctuation level. Similar to electron temperature and diffusion coefficient, the transport time decreases with increasing density fluctuation level, indicating an increased turbulence level. In other words, as the influence of turbulence increases, the impurity confinement diminishes and the transport is enhanced. In particular, the ECRH power appears to have a significant effect on the turbulence level and ultimately on the impurity confinement, although other mechanisms are also important. Figure 5 clearly shows the influence of the ECRH power on the transport time (a) and on the line-averaged diffusion coefficient (b). With increasing heating power, the transport time decreases and the impurity confinement becomes worse, because the turbulence is enhanced, leading to increased turbulent diffusion coefficients. With decreasing ECRH power, the confinement improves as the turbulence is reduced and the transport time increases, the diffusion coefficients are also lower compared with the turbulence enhanced scenario.

https://doi.org/10.1017/S0022377823000417 Published online by Cambridge University Press

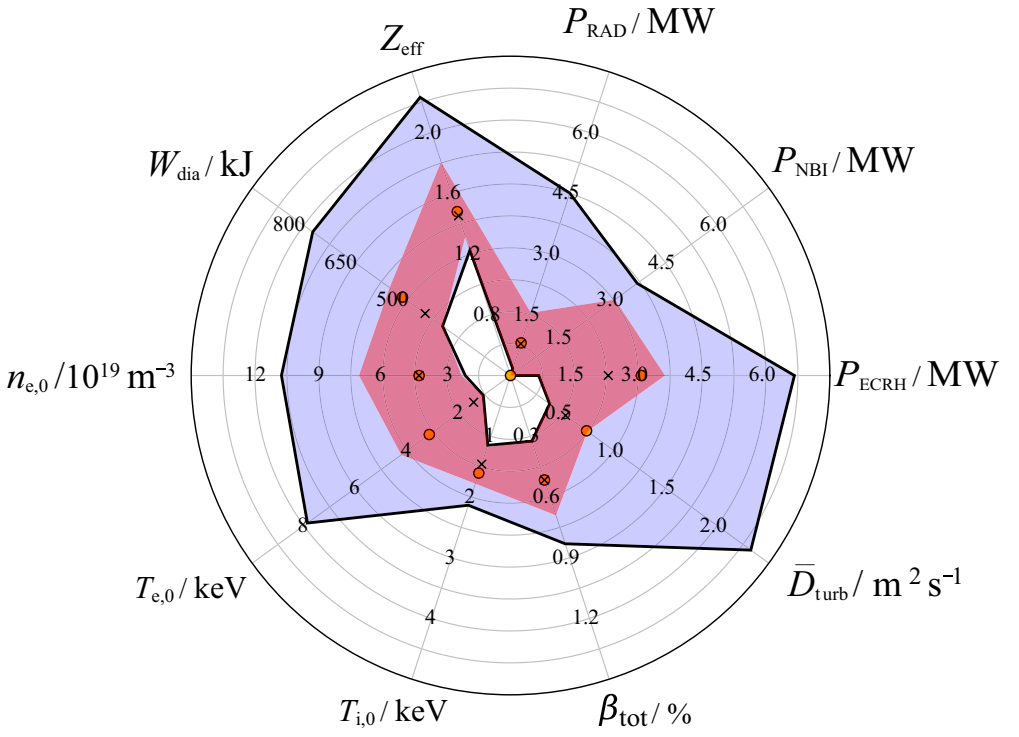

FIGURE 6. Overview of the parameter space of the ECRH power P_{ECRH}, NBI heating power P_{NBI}, radiated power P_{RAD}, effective ion charge Z_{eff}, diamagnetic energy W_{dia}, central values of the electron density $n_{e,0}$, electron temperature $T_{e,0}$ and ion temperature $T_{i,0}$, plasma beta as well as the line-averaged diffusion coefficient. The light blue area represents the whole parameter space as it is shown in figure 1 extended by the diffusion coefficient (median indicated with filled cirlces). The light red area indicates the parameter space for the turbulence reduced scenarios (median indicated with crosses).

The impact of other mechanisms on the impurity confinement will be elaborated in future publications. Especially, the impact of turbulence drivers like the normalized density or temperature gradient length as well as the impact of the electric field will be the focus of upcoming publications. In particular, the scenario with a transport time of approximately 1 s is examined in more detail. With the help of large-scale nonlinear gyro-kinetic simulations, it could be shown that density peaking is the reason for the suppression of turbulence, which leads to a significantly better confinement behavior (Alcusón *et al.* 2023).

Since the level of turbulence strongly regulates the impurity confinement, an overview of the parameter space for the turbulence reduced and enhanced plasma scenarios is given in figure 6. For simplicity, the boundary between these two scenarios is defined here by the transport time. Plasmas with an impurity transport time above 100 ms are assigned to the turbulence reduced scenario, while plasmas with a transport time less than or equal to 100 ms are assigned to the turbulence enhanced scenario. This threshold was selected because the assumption of a completely diffusive transport up to 100 ms transport time is best fulfilled. Further investigations have shown that, above this limit, a convective part is more difficult to neglect. Unfortunately, the current data situation does not allow us to determine the convective part of the transport. Nevertheless, this leads to results that

https://doi.org/10.1017/S0022377823000417 Published online by Cambridge University Press

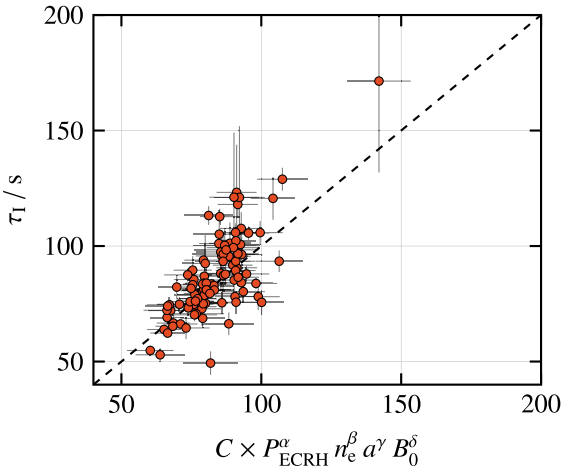

FIGURE 7. Impurity transport time over its value inferred with the scaling law. The axis diagonal is plotted as dotted line.

Fit parameter:	C	α	β	γ	δ
W7-AS	460	-0.8 ± 0.20	1.2 ± 0.20	2.4 ± 0.4	0.3 ± 0.2
W7-X	90	-0.4 ± 0.01	0.2 ± 0.01	0	0

TABLE 1. List of fit parameters of the scaling law $\tau = C \times P_{\mathrm{ECRH}}^{\alpha} \times n_{\mathrm{e},0}^{\beta} \times a^{\gamma} \times B_0^{\delta}$ for W7-AS taken from Burhenn *et al.* (1995) and for W7-X.

describe the experiments well, although the error bars are somewhat larger for plasmas with better impurity confinement.

The attempt to derive scaling laws allows an extrapolation of the impurity transport in future plasma scenarios. Initially, an existing scaling law from W7-AS (Burhenn *et al.* 1995) as the predecessor of W7-X was examined for purely ECRH plasma scenarios as the ECRH power P_{ECRH} is considered only. That scaling law also takes into account the central electron density $n_{\mathrm{e},0}$, minor radius a and the magnetic field strength on axis, B_0. Unfortunately, the parameter space for the minor radius as well magnetic field strength is limited so that no reliable conclusion can be made from this. To derive a reliable scaling law, the data are additionally checked for possible collinearities. The result of that scaling attempt taking into account the database described in § 2 is shown in figure 7. The respective fit parameters and hence the impact strength of the parameter on the confinement behavior are listed in table 1. As already mentioned above, the impact of the ECRH power on the impurity confinement is confirmed also by the scaling attempt in which the exponent of the power is relatively high in absolute value. Additionally, the low exponent of 0.2 is the result of the weak density dependence, as discussed above. Another scaling attempt, which takes into account the drivers for the ion temperature gradient driven turbulent transport, points in the right direction, but cannot yet be shown here because the profile information of the main plasma parameters have to be revised to make trustworthy statements. This will be a topic of future publications.

https://doi.org/10.1017/S0022377823000417 Published online by Cambridge University Press

4. Summary and conclusion

The impurity transport of W7-X under different plasma conditions has been characterized and documented using a database approach. The dependence on plasma parameters has been investigated. Compared with other stellarators, W7-X has only a weak correlation to the electron density. The ECRH power, which also defines the core electron temperature, influences the confinement behavior, which is mainly turbulence dominated. The neoclassical optimization of W7-X (Beidler *et al.* 2021) enables a unique opportunity to observe and document the presence of this turbulent contribution to the overall impurity transport. This is additionally confirmed by scaling attempts taking into account several parameters. This allows an extrapolation of the impurity transport in future plasma scenarios.

The observations shown here are only the beginning and the study of the influence of other parameters will be possible and presented in other publications. In addition, this database will be expanded with data from future campaigns, which will allow monitoring of trends and the integration of other parameters, boundary conditions and magnetic field configurations.

Acknowledgements

Views and opinions expressed are, however, those of the author(s) only and do not necessarily reflect those of the European Union or the European Commission. Neither the European Union nor the European Commission can be held responsible for them.

Editor Cary Forest thanks the referees for their advice in evaluating this article.

Declaration of interest

The authors report no conflict of interest.

Funding

This work has been carried out within the framework of the EUROfusion Consortium, funded by the European Union via the Euratom Research and Training Programme (Grant Agreement No 101052200 - EUROfusion).

REFERENCES

ALCUSÓN, J.A., WEGNER, TH., DINKLAGE, A., LANGENBERG, A., BÄHNER, J.P., BUTTENSCHÖN, B., EDLUND, E.M., FUCHERT, G., GARCÍA-REGAÑA, J.M., GRULKE, O., *et al.* 2023 Quantitative comparison of turbulent impurity transport in turbulence reduced and enhanced scenarios at Wendelstein 7-X. *Nucl. Fusion* (submitted).

ALCUSÓN, J.A., XANTHOPOULOS, P., PLUNK, G.G., HELANDER, P., WILMS, F., TURKIN, Y., VON STECHOW, A. & GRULKE, O. 2020 Suppression of electrostatic micro-instabilities in maximum-J stellarators. *Plasma Phys. Control. Fusion* **62** (3), 035005.

ANDREEVA, T. 2002 Vacuum magnetic configurations of Wendelstein 7-X. IPP III/270. Max-Planck-Institut für Plasmaphysik.

BEHRINGER, K. 1987 Description of the impurity transport code "STRAHL". JET Joint Undertaking.

BEIDLER, C.D., SMITH, H.M., ALONSO, J.A., ANDREEVA, T., BALDZUHN, J., BEURSKENS, M.N.A., BOZHENKOV, S.A., BRUNNER, K.J., DAMM, H., DREVLAK, M., *et al.* 2021 Demonstration of reduced neoclassical energy transport in Wendelstein 7-X. *Nature* **596** (7871), 221–226.

BEURSKENS, M.N.A., BOZHENKOV, S.A., FORD, O., XANTHOPOULOS, P., ZOCCO, A., TURKIN, Y., ALONSO, J.A., BEIDLER, C., CALVO, I., CARRALERO, D., *et al.* 2021 Ion temperature clamping in Wendelstein 7-X electron cyclotron heated plasmas. *Nucl. Fusion* **61** (11), 116072.

https://doi.org/10.1017/S0022377823000417 Published online by Cambridge University Press

Burhenn, R., Feng, Y., Ida, K., Maassberg, H., McCarthy, K.J., Kalinina, D., Kobayashi, M., Morita, S., Nakamura, Y., Nozato, H., *et al.* 2009 On impurity handling in high performance stellarator/heliotron plasmas. *Nucl. Fusion* **49** (6), 065005.

Burhenn, R., Hacker, H., Ledl, L., Unger, E., Baldzuhn, J., Hofmann, J.V. & Weller, A. 1995 Transport studies of injected impurities in the stellarator Wendelstein 7-AS. In *Proceedings of the 22nd Conference on Controlled Fusion and Plasma Physics, Part III*, vol. 19C, p. 145. European Physical Society.

Edlund, E.M., Porkolab, M., Huang, Z., Grulke, O., Böttger, L.-G., von Sehren, C. & von Stechow, A. 2018 Overview of the Wendelstein 7-X phase contrast imaging diagnostic. *Rev. Sci. Instrum.* **89** (10), 10E105.

García-Regaña, J.M., Barnes, M., Calvo, I., González-Jerez, A., Thienpondt, H., Sánchez, E., Parra, F.I. & St-Onge, D.A. 2021*a* Turbulent transport of impurities in 3D devices. *Nucl. Fusion* **61** (11), 116019.

García-Regaña, J.M., Barnes, M., Calvo, I., Parra, F.I., Alcusón, J.A., Davies, R., González-Jerez, A., Mollén, A., Sánchez, E., Velasco, J.L., *et al.* 2021*b* Turbulent impurity transport simulations in Wendelstein 7-X plasmas. *J. Plasma Phys.* **87** (1), 855870103.

Geiger, B., Wegner, Th., Beidler, C.D., Burhenn, R., Buttenschön, B., Dux, R., Langenberg, A., Pablant, N.A., Pütterich, T., Turkin, Y., *et al.* 2019 Observation of anomalous impurity transport during low-density experiments in W7-X with laser blow-off injections of iron. *Nucl. Fusion* **59** (4), 046009.

Helander, P. & Zocco, A. 2018 Quasilinear particle transport from gyrokinetic instabilities in general magnetic geometry. *Plasma Phys. Control. Fusion* **60** (8), 084006.

Hirshman, S.P., Shaing, K.C., van Rij, W.I., Beasley, C.O. & Crume, E.C. 1986 Plasma transport coefficients for nonsymmetric toroidal confinement systems. *Phys. Fluids* **29** (9), 2951–2959.

Ida, K., Fonck, R.J., Sesnic, S., Hulse, R.A. & LeBlanc, B. 1987 Observation of Z-dependent impurity accumulation in the pbx tokamak. *Phys. Rev. Lett.* **58**, 116–119.

Klinger, T., Andreeva, T., Bozhenkov, S.A., Brandt, C., Burhenn, R., Buttenschön, B., Fuchert, G., Geiger, B., Grulke, O., Laqua, H.P., *et al.* 2019 Overview of first Wendelstein 7-X high-performance operation. *Nucl. Fusion* **59** (11), 112004.

Langenberg, A., Pablant, N.A., Marchuk, O., Zhang, D., Alonso, J.A., Burhenn, R., Svensson, J., Valson, P., Gates, D., Beurskens, M.N.A., *et al.* 2017 Argon impurity transport studies at Wendelstein 7-X using x-ray imaging spectrometer measurements. *Nucl. Fusion* **57** (8), 086013.

Langenberg, A., Wegner, Th., Marchuk, O., García-Regaña, J.M., Pablant, N.A., Fuchert, G., Bozhenkov, S.A., Damm, H., Pasch, E., Brunner, K.J., *et al.* 2021 Impurity transport in ion- and electron-root confinement scenarios at Wendelstein 7-X. *Nucl. Fusion* **61** (11), 116018.

Langenberg, A., Wegner, Th., Pablant, N.A., Marchuk, O., Geiger, B., Tamura, N., Bussiahn, R., Kubkowska, M., Mollén, A., Traverso, P., *et al.* 2020 Charge-state independent anomalous transport for a wide range of different impurity species observed at Wendelstein 7-X. *Phys. Plasmas* **27** (5), 052510.

Navarro, A.B., Merlo, G., Plunk, G.G., Xanthopoulos, P., von Stechow, A., Siena, A.D., Maurer, M., Hindenlang, F., Wilms, F. & Jenko, F. 2020 Global gyrokinetic simulations of ITG turbulence in the magnetic configuration space of the Wendelstein 7-X stellarator. *Plasma Phys. Control. Fusion* **62** (10), 105005.

Pasch, E., Beurskens, M.N.A., Bozhenkov, S.A., Fuchert, G., Knauer, J. & Wolf, R.C. 2016 The thomson scattering system at Wendelstein 7-X. *Rev. Sci. Instrum.* **87** (11), 11E729.

Romba, T., Reimold, F., Ford, O.P., Jaspers, R.J.E., Vanó, L. & Klinger, T. 2023 Suppression of anomalous impurity transport in NBI-heated W7-X plasmas. *Nucl. Fusion* (submitted).

Wegner, Th., Alcusón, J.A., Geiger, B., von Stechow, A., Xanthopoulos, P., Angioni, C., Beurskens, M.N.A., Böttger, L.-G., Bozhenkov, S.A., Brunner, K.J., *et al.* 2020*a* Impact of the temperature ratio on turbulent impurity transport in Wendelstein 7-X. *Nucl. Fusion* **60**, 124004.

WEGNER, TH., GEIGER, B., FOEST, R., VAN VUUREN, A.J., WINTERS, V.R., BIEDERMANN, C., BURHENN, R., BUTTENSCHÖN, B., CSEH, G., JODA, I., *et al.* 2020*b* Preparation, analysis, and application of coated glass targets for the Wendelstein 7-X laser blow-off system. *Rev. Sci. Instrum.* **91** (8), 083503.

WEGNER, TH., GEIGER, B., KUNKEL, F., BURHENN, R., SCHRÖDER, T., BIEDERMANN, C., BUTTENSCHÖN, B., CSEH, G., DREWS, P., GRULKE, O., *et al.* 2018 Design, capabilities, and first results of the new laser blow-off system on Wendelstein 7-X. *Rev. Sci. Instrum.* **89** (7), 073505.

XANTHOPOULOS, P., BOZHENKOV, S.A., BEURSKENS, M.N.A., SMITH, H.M., PLUNK, G.G., HELANDER, P., BEIDLER, C.D., ALCUSÓN, J.A., ALONSO, J.A. & DINKLAGE, A. 2020 Turbulence mechanisms of enhanced performance stellarator plasmas. *Phys. Rev. Lett.* **125**, 075001.

https://doi.org/10.1017/S0022377823000417 Published online by Cambridge University Press